Journal of
Applied Crystallography
ISSN 0021-8898
Editor: **Anke R. Kaysser-Pyzalla**

Application of a theory for particle statistics to structure refinement from powder diffraction data

T. Ida and F. Izumi

J. Appl. Cryst. (2011). **44**, 921–927

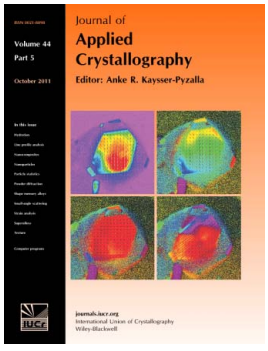

Journal of
Applied Crystallography
ISSN 0021-8898

Received 17 June 2011
Accepted 2 August 2011

Application of a theory for particle statistics to structure refinement from powder diffraction data

T. Ida[a]* and F. Izumi[a,b]

[a]Ceramics Research Laboratory, Nagoya Institute of Technology, Asahigaoka 10-6-29, Tajimi, Gifu 507-0071, Japan, and [b]Quantum Beam Unit, National Institute for Materials Science, 1-1 Namiki, Tsukuba, Ibaraki 305-0044, Japan. Correspondence e-mail: ida.takashi@nitech.ac.jp

A new methodology is proposed for structure refinement using powder diffraction data, from which models for particle statistics and any other statistical errors can be formally optimized. This method is nothing but a straightforward implementation of the maximum-likelihood method, extended to the error estimation. Structure parameters refined by the method for fluorapatite [$Ca_5(PO_4)_3F$], anglesite ($PbSO_4$) and barite ($BaSO_4$) become significantly closer to those obtained by single-crystal structure analyses in comparison with the results of the conventional Rietveld method.

1. Introduction

The analysis of powder diffraction intensities generally assumes a sufficiently large number of crystallites that satisfy the diffraction condition. However, this assumption no longer holds if the crystallites in a powder sample are not small enough and/or if the diffractometer has high angular resolution.

A theory on particle statistics in powder diffraction measurements for stationary specimens in a symmetric reflection mode was established by the pioneering work of Alexander *et al.* (1948) and extended to rotating specimens by De Wolff (1958). Experimental errors arising from particle statistics in crystalline powders with particle sizes of several micrometres were shown to be comparable to those caused by counting statistics about intensity data measured under typical experimental conditions (Alexander *et al.*, 1948).

Ida *et al.* (2009) have recently found that the effect of particle statistics can be evaluated quantitatively by analysing diffraction intensities observed in step-scan measurements about the rotation angle of the sample spinner attached to a laboratory powder diffractometer. They concluded that intensity data resulting from the spinner-scan measurements include information about the texture of the specimen and that crystallite sizes of about several micrometres can be determined by the method. However, the method is practically useless for application to structure analysis because it only gives particle statistics about stationary specimens. There is no reason not to apply continuous rotation of the specimen to data collection for structure analysis when a sample spinner is attached to the diffractometer.

In this study, a new methodology is proposed for structure refinement using powder diffraction data, from which models for particle statistics and any other statistical errors can be formally optimized. The method is only a straightforward implementation of the maximum-likelihood estimation (Antoniadis *et al.*, 1990), extended to the error estimation. The validity of our analytical method has been examined by its applications to standard powder diffraction data of fluorapatite [$Ca_5(PO_4)_3F$], anglesite ($PbSO_4$) and barite ($BaSO_4$).

2. Theoretical

Suppose that diffraction intensities $\{Y_j\}$ observed at diffraction angles $\{2\Theta_j\}$ are normally distributed around the true model $\{y(2\Theta_j)\}$ with a statistical error of $\{\sigma_j\}$ at each data point. Then the probability that this data set is realized is given by

$$P = \prod_{j=1}^{N} \frac{1}{(2\pi)^{1/2}\sigma_j} \exp\left\{-\frac{[Y_j - y(2\Theta_j)]^2}{2\sigma_j^2}\right\}. \quad (1)$$

The maximum-likelihood estimation is equivalent to the minimization of the negative of the logarithm of the above probability:

$$-\ln P = \frac{N}{2}\ln(2\pi) + \frac{1}{2}\sum_{j=1}^{N}\left(\ln\sigma_j^2 + \frac{\Delta_j^2}{\sigma_j^2}\right), \quad (2)$$

where $\Delta_j \equiv Y_j - y(2\Theta_j)$.

The total statistical variance σ_j^2 is modelled by the sum of the variance caused by counting statistics $(\sigma_c)_j^2$ and particle statistics $(\sigma_p)_j^2$ in powder diffractometry, that is,

$$\sigma_j^2 \simeq (\sigma_c)_j^2 + (\sigma_p)_j^2. \quad (3)$$

The variance caused by counting statistics is naturally approximated by the expected value of the number of observed X-ray photons,

$$(\sigma_c)_j^2 \simeq y(2\Theta_j), \quad (4)$$

in measurements involving a counting method because the counting event should follow Poisson statistics when the counting loss is negligible (Ida, 2008).

The dependence of the variance caused by particle statistics on the diffraction angle 2Θ varies with the geometry of the diffractometer. The formula for the symmetric reflection (Bragg–Brentano) geometry is given by

$$(\sigma_{\rm p})_j^2 \propto [y(2\Theta_j) - b_j]^2 \sin\Theta_j/(m_{\rm eff})_j \quad (5)$$

for stationary specimens (Alexander *et al.*, 1948) and

$$(\sigma_{\rm p})_j^2 \propto [y(2\Theta_j) - b_j]^2 \sin^2\Theta_j/(m_{\rm eff})_j \quad (6)$$

for rotating (spinning) specimens (De Wolff, 1958), where b_j is the background intensity. $(m_{\rm eff})_j$ is the effective multiplicity, defined for overlapped reflections with the component multiplicity m_k and the Bragg diffraction intensity I_k by the following equation (Ida *et al.*, 2009):

$$(m_{\rm eff})_j = \left(\sum_k m_k I_k\right)^2 \Big/ \sum_k m_k I_k^2. \quad (7)$$

Recently, we have also proposed a formula of particle statistics for capillary transmission measurements, minimizing (Ida, 2011)

$$(\sigma_{\rm p})_j^2 \propto \frac{[y(2\Theta_j) - b_j]^2 A(2\mu R, \Theta_j)\sin\Theta_j}{(m_{\rm eff})_j [A(\mu R, \Theta_j)]^2}, \quad (8)$$

where $A(\mu R, \theta)$ is the overall transmittance at 2θ for a cylindrical sample with a linear absorption coefficient μ and a radius R.

The proportionality factors in equations (5), (6) and (8) depend on the spectroscopic distribution of source X-rays, the dimensions of the optics, the effective crystallite size and the absorption coefficient of the specimen. In our methodology, these factors are regarded as unknown parameters to be optimized from powder diffraction data measured experimentally, simply by minimizing equation (2) or the function

$$S = \sum_{j=1}^{N} \left(\ln \sigma_j^2 + \Delta_j^2/\sigma_j^2\right). \quad (9)$$

Note that, in conventional Rietveld (1969) analysis, $\sum_j \Delta_j^2/\sigma_j^2$ is merely minimized by nonlinear least-squares methods on the assumption that all the values of errors $\{\sigma_j\}$ are known *a priori*.

In principle, any models for statistical errors can be optimized by minimizing S in equation (9). In the present study, we restrict our attention to measurements using the stationary-specimen symmetric reflection mode [see equation (5)], incorporating another term into the error model:

$$\sigma_j^2 = (\sigma_{\rm c})_j^2 + (\sigma_{\rm p})_j^2 + (\sigma_{\rm r})_j^2, \quad (10)$$

$$(\sigma_{\rm p})_j^2 = C_{\rm p}[y(2\Theta_j) - b_j]^2 \sin\Theta_j/(m_{\rm eff})_j, \quad (11)$$

$$(\sigma_{\rm r})_j^2 = C_{\rm r}[y(2\Theta_j)]^2, \quad (12)$$

where the two proportionality factors, $C_{\rm p}$ and $C_{\rm r}$, are variable parameters to be optimized. The term defined by equation (12) is mainly intended to represent deviations caused by the incompleteness of the profile model. Toraya (1998, 2000) also suggested the existence of statistical errors proportional to observed intensities. Comparison of $C_{\rm p}$ with $C_{\rm r}$ is expected to provide information about the contribution of particle statistics to the source diffraction data.

3. Analytical procedures

The following procedures are applied to structure refinement.

(i) A conventional Rietveld refinement is applied to powder diffraction data, with initial statistical errors of $\sigma_j = Y_j^{1/2}$.

(ii) An individual diffraction peak profile $f_k(2\Theta_j)$, which corresponds to $m_k I_k$ in equation (7), is extracted on the final calculation of the optimized diffraction intensity in the Rietveld analysis. Then the effective multiplicity at each data point is calculated by

$$(m_{\rm eff})_j = \frac{\left[\sum_k f_k(2\Theta_j)\right]^2}{\sum_k [f_k(2\Theta_j)]^2/m_k} \quad (13)$$

for the component multiplicity m_k.

(iii) The two-dimensional function $S(C_{\rm p}, C_{\rm r})$ in equations (9) and (10) is minimized in the $(C_{\rm p}, C_{\rm r})$ plane under inequality constraints of $0 < C_{\rm p}$ and $0 < C_{\rm r}$ by a downhill simplex (Nelder–Mead) algorithm (Press *et al.*, 2007). Initial vertices are chosen at $(C_{\rm p}, C_{\rm r}) = (10^{-5}, 10^{-5})$, $(1, 10^{-5})$ and $(10^{-5}, 1)$.

(iv) A further Rietveld refinement is carried out with the statistical error σ_j calculated by equation (10) at each data point, and then steps (ii)–(iv) are repeated until convergence.

4. Applications to X-ray powder diffraction data

The results of Rietveld analysis and the new analytical method on powder diffraction data of fluorapatite [$Ca_5(PO_4)_3F$], anglesite ($PbSO_4$) and barite ($BaSO_4$), measured with Bragg–Brentano diffractometers, are demonstrated in this section. The Rietveld analysis program *RIETAN-FP* (version 2.0; Izumi & Momma, 2007) was used for all the Rietveld refinements in this study. The scale factor, a constant peak-shift parameter, a ninth-order polynomial for the background intensity, and the profile parameters of a split pseudo-Voigt function (Toraya, 1990) were optimized during the structure refinements. Corrections for preferred orientation or surface roughness were not applied.

4.1. Fluorapatite, $Ca_5(PO_4)_3F$

X-ray powder diffraction data of fluorapatite, $Ca_5(PO_4)_3F$, measured with Cu $K\alpha$ radiation, were originally attached to the *DBWS* Rietveld program package developed by Young *et al.* (1995) and are currently available as an example data set in the *RIETAN-FP* package (Izumi & Momma, 2007). The space group of $Ca_5(PO_4)_3F$ is $P6_3/m$ (No. 176). In our structure refinement from the powder diffraction data, the atomic

scattering factors of F^-, Ca^{2+}, P and O^- were used, similarly to a single-crystal X-ray analysis (Sudarsanan *et al.*, 1972). The occupancies of all the sites were not optimized but fixed at unity in the analysis of the powder diffraction data.

Fig. 1 illustrates a contour map of the function $S(C_p, C_r)$ defined by equation (9) and the location of its minimum after the third iteration, where no further changes in structure parameters were detected. It can be seen from Fig. 1 that C_p and C_r show a strong negative correlation with each other.

Effective multiplicities, $(m_{eff})_j$, calculated with equation (7) are plotted against 2Θ in Fig. 2. The effective multiplicity exhibits complicated behaviour but generally tends to have larger values in the higher-angle region, presumably as a result

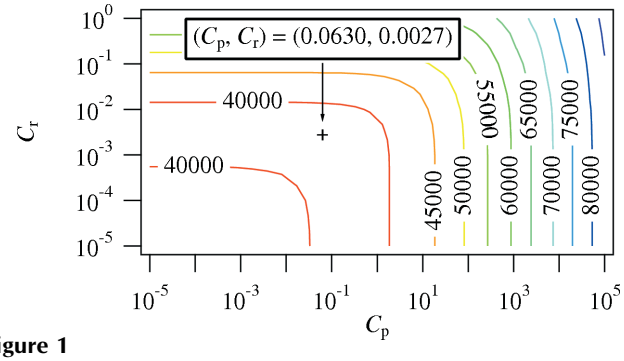

Figure 1
Contour map and the minimum position of the two-dimensional function $S(C_p, C_r)$, defined by equation (9), for $Ca_5(PO_4)_3F$.

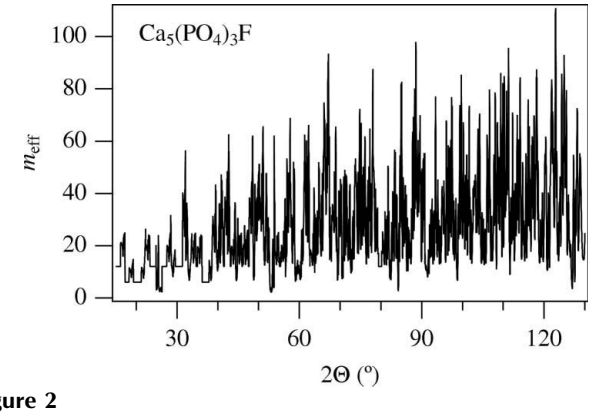

Figure 2
Effective multiplicity m_{eff} *versus* 2Θ for $Ca_5(PO_4)_3F$.

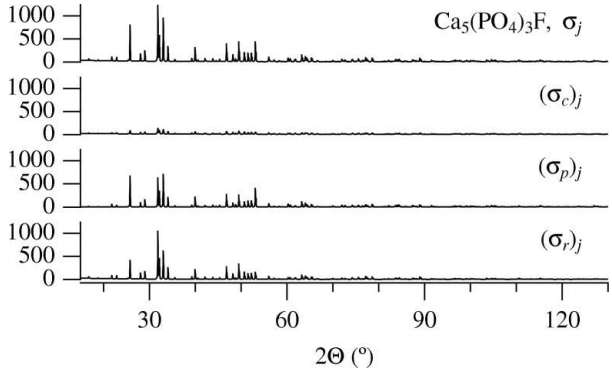

Figure 3
Total and component errors estimated for $Ca_5(PO_4)_3F$.

Table 1
Structure parameters of fluorapatite, $Ca_5(PO_4)_3F$, optimized by the Rietveld analysis, final values on convergence of the iterative calculations incorporating the error model for particle statistics, and structure data obtained by the single-crystal method for the mineral and synthetic crystals (Sudarsanan *et al.*, 1972).

	Rietveld	New method	Mineral	Synthetic
R_{wp} (%)	8.20	9.17		
R_p (%)	6.42	6.76		
R_e (%)	5.59	9.23		
S	1.467	0.993		
a (Å)	9.37127 (10)	9.37124 (11)	9.363 (2)	9.367 (1)
c (Å)	6.88549 (6)	6.88547 (7)	6.878 (2)	6.884 (1)
F: g	1	1	0.906 (6)	0.942 (4)
F: x	0	0	0	0
F: y	0	0	0	0
F: z	1/4	1/4	1/4	1/4
F: B (Å^2)	1.31 (9)	1.80 (11)	1.24 (3)	1.25 (2)
Ca1: g	1	1	0.990 (3)	0.942 (4)
Ca1: x	1/3	1/3	1/3	1/3
Ca1: y	2/3	2/3	2/3	2/3
Ca1: z	0.012 (2)	0.0012 (2)	0.0012 (1)	0.0011 (0)
Ca1: B (Å^2)	0.69 (2)	0.73 (3)	0.59 (1)	0.65 (0)
Ca2: g	1	1	0.986 (2)	0.976 (2)
Ca2: x	0.24185 (12)	0.24169 (14)	0.2415 (1)†	0.2416 (0)†
Ca2: y	0.24961 (12)	0.24908 (13)	0.2486 (1)†	0.2487 (0)†
Ca2: z	1/4	1/4	1/4	1/4
Ca2: B (Å^2)	0.58 (2)	0.57 (2)	0.50 (2)	0.51 (1)
P: g	1	1	1.008 (2)	0.992 (2)
P: x	0.39719 (16)	0.39795 (17)	0.3982 (1)	0.3981 (0)
P: y	0.02936 (16)	0.02933 (17)	0.0293 (1)	0.0293 (0)
P: z	1/4	1/4	1/4	1/4
P: B (Å^2)	0.57 (3)	0.51 (3)	0.45 (2)	0.33 (0)
O1: g	1	1	0.990 (3)	0.975 (3)
O1: x	0.1599 (3)	0.1593 (4)	0.1582 (1)	0.1581 (1)
O1: y	0.4848 (3)	0.4833 (4)	0.4850 (1)	0.4843 (1)
O1: z	1/4	1/4	1/4	1/4
O1: B (Å^2)	0.66 (7)	0.75 (7)	0.75 (2)	0.70 (1)
O2: g	1	1	0.986 (2)	0.976 (2)
O2: x	0.5912 (4)	0.5896 (4)	0.5881 (1)	0.5880 (1)
O2: y	0.1215 (4)	0.1211 (5)	0.1213 (1)	0.1212 (1)
O2: z	1/4	1/4	1/4	1/4
O2: B (Å^2)	0.70 (7)	0.92 (8)	0.92 (2)	0.83 (1)
O3: g	1	1	0.988 (4)	1.000 (6)
O3: x	0.3394 (3)	0.3408 (4)	0.3415 (1)	0.3416 (1)
O3: y	0.0815 (2)	0.0832 (3)	0.0846 (1)	0.0848 (1)
O3: z	0.0706 (3)	0.0708 (4)	0.0704 (1)	0.0704 (1)
O3: B (Å^2)	0.77 (5)	0.91 (5)	1.03 (2)	0.93 (1)

† Corrected and standardized values.

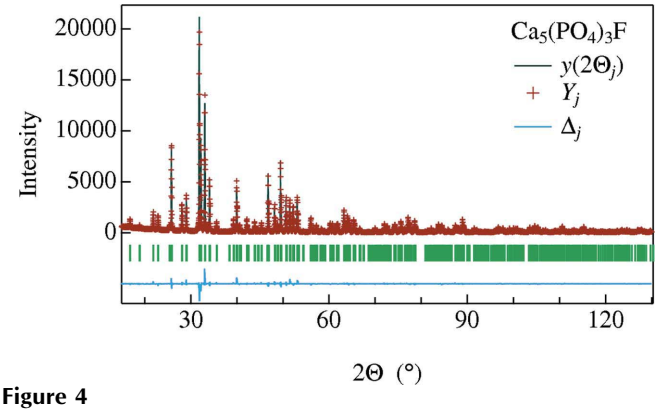

Figure 4
Final results of curve fitting for $Ca_5(PO_4)_3F$.

of heavier overlap of reflections. This finding suggests that errors arising from particle statistics are estimated at smaller values in the higher-angle region, and partly compensate the increasing factor of $\sin\Theta$ for stationary specimens in equation (11).

Fig. 3 shows calculated total errors σ_j and their components, $(\sigma_c)_j$, $(\sigma_p)_j$ and $(\sigma_r)_j$, which are, respectively, counting statistical, particle statistical and additional errors. The values estimated for $(\sigma_p)_j$ and $(\sigma_r)_j$ are very similar to each other and clearly larger than the counting statistical errors $(\sigma_c)_j$ for this data set.

The results of the final curve fitting to the observed powder diffraction data are plotted in Fig. 4. Table 1 lists reliability factors and structure parameters refined by the Rietveld and new analytical methods, including structure parameters optimized by single-crystal X-ray analyses of mineral and synthetic fluorapatite (Sudarsanan *et al.*, 1972). The fractional coordinates in Table 1 were standardized with *STRUCTURE TIDY* (Gelato & Parthé, 1987) executed from the three-dimensional visualization system *VESTA* (Momma & Izumi, 2008). The z value of atom O3 was revised from the value of 0.00704 (1) reported in the literature (Sudarsanan *et al.*, 1972) to −0.00704 (1) before the standardization, because a fit to the powder diffraction data with the original value was very poor while that with the corrected value was satisfactory.

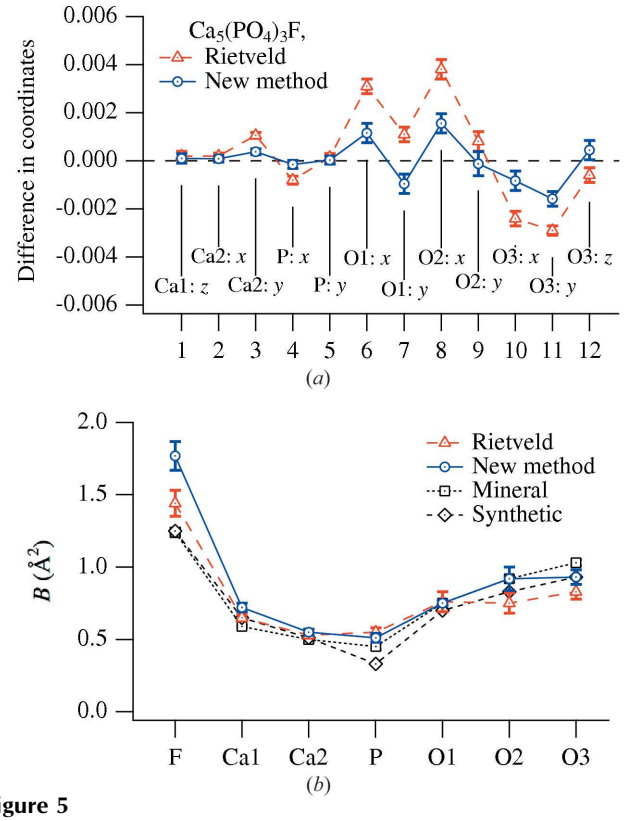

Figure 5
(*a*) Deviations of the fractional coordinates optimized by the Rietveld and new methods (which are, respectively, marked with triangles and circles) from those for the synthetic single crystal for $Ca_5(PO_4)_3F$. (*b*) Isotropic atomic displacement parameters optimized by the Rietveld and new methods (triangles and circles, respectively) and equivalent isotropic atomic displacement parameters obtained with the mineral and synthetic single crystals (which are, respectively, marked with squares and diamonds) for $Ca_5(PO_4)_3F$ (Sudarsanan *et al.*, 1972).

(*a*) The differences in atomic coordinates between the structure refinements from the powder and single-crystal diffraction data, and (*b*) isotropic atomic displacement parameters, B, refined from the powder data and the equivalent isotropic atomic displacement parameters, B_{eq}, refined from the single-crystal data are plotted in Figs. 5(*a*) and 5(*b*), respectively. All the atomic fractional coordinates optimized by our new method were closer to the single-crystal data than those obtained by the Rietveld method. The unusually large B(F) parameter resulting from our new method may be ascribed to the slight deficiency of the F site, which was pointed out by Sudarsanan *et al.* (1972).

It should be noted that R_p in the new analytical method was larger than that in the Rietveld analysis, which means that the new method relies less on the coincidence with the observed profile than the Rietveld method. We should be careful about this habit of the new method, although it seems to work well in this particular case.

4.2. Anglesite, $PbSO_4$

X-ray powder diffraction data of anglesite, $PbSO_4$, supplied for a Rietveld refinement round robin (Hill, 1992), were reanalysed in this study. The data are available as an example file in the *FullProf* package (Rodriguez-Carvajal, 1993). The space group of $PbSO_4$ is *Pnma* (No. 62). Atomic scattering factors for neutral atoms were used for our structure refinements, similarly to a single-crystal X-ray analysis by Miyake *et al.* (1978).

Fig. 6 illustrates a contour map of $S(C_p, C_r)$ and the position of its minimum on convergence after the third iteration cycle of the new analytical method. Effective multiplicities for $PbSO_4$ data are plotted against 2Θ in Fig. 7.

Fig. 8 shows calculated total errors σ_j and components $(\sigma_c)_j$, $(\sigma_p)_j$ and (σ_r) for $PbSO_4$. Estimated values about $(\sigma_r)_j$ were found to be larger than those for $(\sigma_p)_j$, which suggests that the errors caused by particle statistics are not dominant in this data set.

The results of the final curve fitting to the powder diffraction data are plotted in Fig. 9. Table 2 lists reliability factors and structure parameters optimized by the Rietveld and new methods. Standardized structure parameters refined by single-

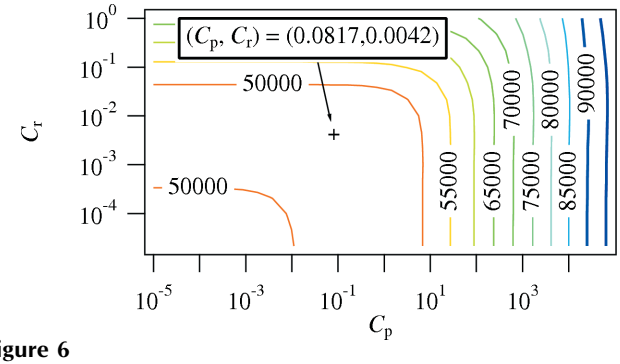

Figure 6
Contour map and the minimum position of $S(C_p, C_r)$ for $PbSO_4$.

Table 2
Structure parameters of anglesite, $PbSO_4$, optimized by the Rietveld method, new analytical method and single-crystal methods (Miyake *et al.*, 1978; Lee *et al.*, 2005).

	Rietveld	New method	Miyake *et al.* (1978)	Lee *et al.* (2005)
R_{wp} (%)	8.70	9.66		
R_p (%)	6.44	7.15		
R_e (%)	4.93	9.43		
S	1.765	1.024		
a (Å)	8.48085 (11)	8.48032 (13)	8.482 (2)	8.475 (2)
b (Å)	5.39895 (8)	5.39842 (9)	5.398 (2)	5.3960 (10)
c (Å)	6.96053 (10)	6.96016 (11)	6.959 (2)	6.9500 (10)
Pb: x	0.18786 (8)	0.18783 (10)	0.1879 (1)	0.1879 (1)
Pb: y	1/4	1/4	1/4	1/4
Pb: z	0.66734 (11)	0.66718 (14)	0.6667 (1)	0.6672 (1)
Pb: B (Å^2)	1.524 (19)	1.49 (2)	1.48 (3)	1.88 (4)
S: x	0.0644 (5)	0.0645 (6)	0.0633 (6)	0.0641 (3)
S: y	1/4	1/4	1/4	1/4
S: z	0.1843 (6)	0.1845 (7)	0.1842 (7)	0.1844 (4)
S: B (Å^2)	1.52 (2)	0.86 (9)	0.74 (7)	1.68 (9)
O1: x	0.4060 (10)	0.4049 (15)	0.408 (2)	0.4071 (11)
O1: y	1/4	1/4	1/4	1/4
O1: z	0.4030 (12)	0.4030 (16)	0.404 (3)	0.4044 (14)
O1: B (Å^2)	0.8 (2)	0.9 (2)	1.9 (4)	2.9 (2)
O2: x	0.1871 (12)	0.1871 (15)	0.194 (2)	0.1928 (10)
O2: y	1/4	1/4	1/4	1/4
O2: z	0.0417 (15)	0.040 (2)	0.043 (2)	0.0407 (14)
O2: B (Å^2)	1.4 (2)	1.6 (3)	1.8 (4)	2.2 (2)
O3: x	0.0802 (7)	0.0814 (10)	0.082 (1)	0.0813 (7)
O3: y	0.0284 (10)	0.0255 (15)	0.026 (2)	0.0257 (12)
O3: z	0.3121 (10)	0.3101 (12)	0.309 (2)	0.3094 (14)
O3: B (Å^2)	1.10 (14)	1.02 (17)	1.3 (2)	2.2 (1)

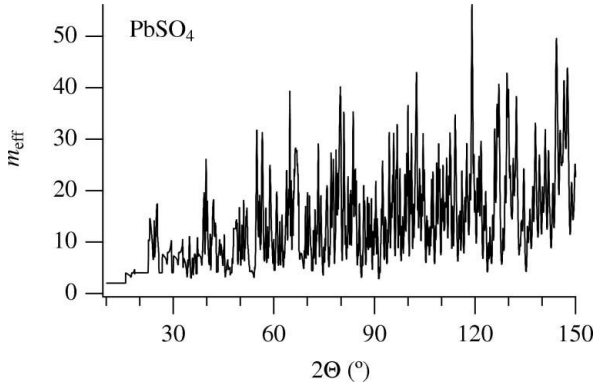

Figure 7
Effective multiplicity m_{eff} *versus* 2Θ for $PbSO_4$.

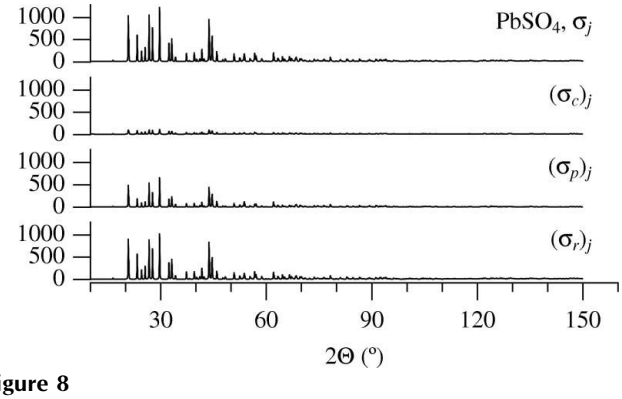

Figure 8
Total and component errors estimated for $PbSO_4$.

crystal X-ray analyses (Miyake *et al.*, 1978; Lee *et al.*, 2005) are also listed in the table. Miyake *et al.* (1978) used a lamellar crystal of anglesite with dimensions of 0.17 × 0.17 × 0.03 mm, collected 749 independent diffraction data with a four-circle diffractometer with Mo $K\alpha$ radiation, and optimized the structure parameters with R = 6.7%. Lee *et al.* (2005) used a crystal with dimensions of 0.1 × 0.08 × 0.06 mm, collected diffraction data of 396 independent reflections with a Bruker

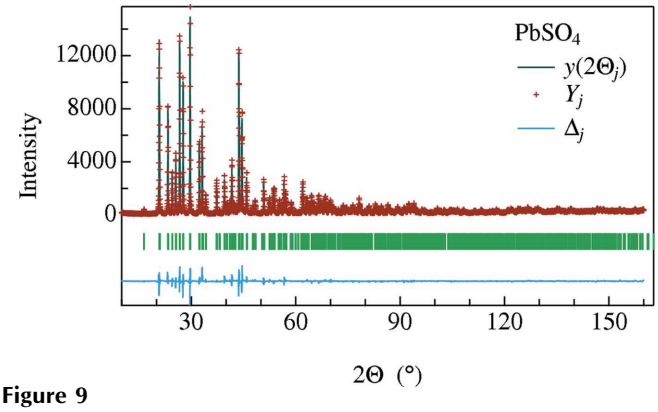

Figure 9
Final results of curve fitting for $PbSO_4$.

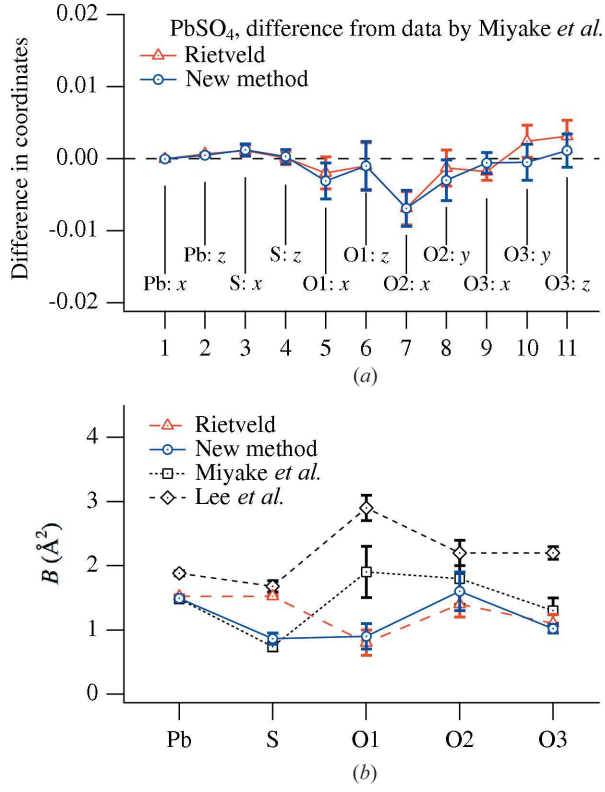

Figure 10
(*a*) Deviation of the fractional coordinates optimized by the Rietveld and new methods (respectively, marked by triangles and circles) from those obtained by the single-crystal X-ray analysis by Miyake *et al.* (1978) for $PbSO_4$. (*b*) Isotropic displacement parameters optimized by the Rietveld and new methods (triangles and circles) and equivalent isotropic displacement parameters calculated from the single-crystal data (Miyake *et al.*, 1978; Lee *et al.*, 2005).

SMART CCD diffractometer with Mo $K\alpha$ radiation, and optimized the structure parameters with an overall $R = 4.27\%$.

(*a*) The differences in atomic coordinates between the structure refinements from the powder data by the Rietveld and new analytical methods and those from single-crystal data (Miyake *et al.*, 1978), and (*b*) isotropic atomic displacement parameters, B, optimized from the powder data and equivalent isotropic displacement parameters, B_{eq}, calculated from the single-crystal data are plotted in Figs. 10(*a*) and 10(*b*), respectively. Though the data obtained by the new analytical method are not far from those resulting from the Rietveld analysis, the coordinates of atom O3 and B(S) are clearly closer to those obtained by the single-crystal analysis by Miyake *et al.* (1978).

4.3. Barite, $BaSO_4$

X-ray powder diffraction data of barite, $BaSO_4$, measured with Cu $K\alpha_1$ radiation, are supplied as an example data file in the *RIETAN-FP* package (Izumi & Momma, 2007). Barite is isostructural to anglesite, with a space group of *Pnma* (No. 62). Atomic scattering factors for neutral atoms were used for structure refinements from the powder data, similarly to a single-crystal X-ray analysis by Miyake *et al.* (1978).

Fig. 11 illustrates a contour map of $S(C_p, C_r)$ and the location of its minimum after the third iteration cycle of the new analytical method. The value of C_r converged at zero in every iteration cycle, which implies that errors caused by particle statistics are intrinsically dominant in this data set.

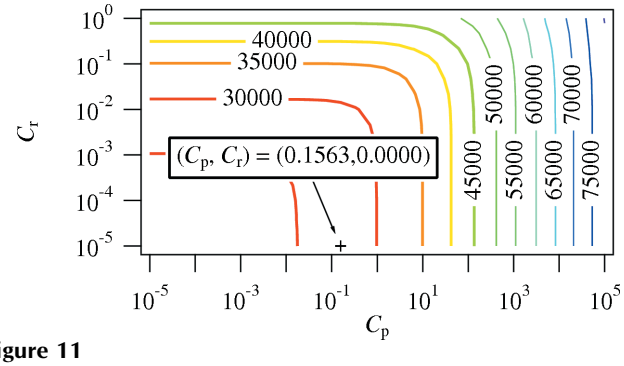

Figure 11
Contour map and the minimum position of S for $BaSO_4$.

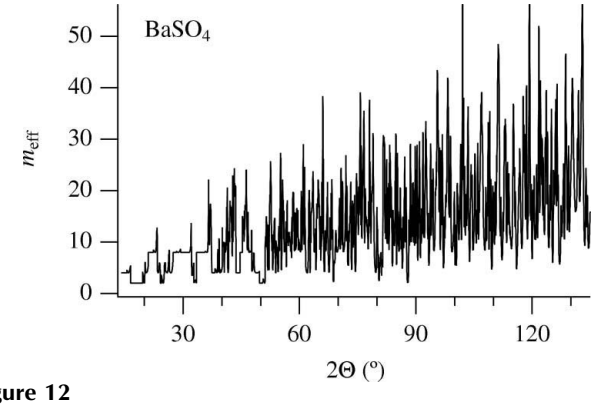

Figure 12
Effective multiplicity m_{eff} *versus* 2Θ for $BaSO_4$.

Table 3
Structure parameters of barite, $BaSO_4$, optimized by the Rietveld method, new analytical method and single-crystal methods (Miyake *et al.*, 1978; Lee *et al.*, 2005).

	Rietveld	New method	Miyake *et al.* (1978)	Lee *et al.* (2005)
R_{wp} (%)	12.34	12.81		
R_p (%)	9.66	10.18		
R_e (%)	10.27	15.27		
S	1.202	1.839		
a (Å)	8.87539 (12)	8.87506 (11)	8.884 (2)	8.896 (1)
b (Å)	5.45216 (7)	5.45198 (7)	5.457 (3)	5.462 (1)
c (Å)	7.15275 (10)	7.15255 (9)	7.157 (2)	7.171 (1)
Ba: x	0.18443 (9)	0.18446 (8)	0.1845 (1)	0.1845 (1)
Ba: y	1/4	1/4	1/4	1/4
Ba: z	0.65894 (12)	0.65867 (11)	0.6585 (1)	0.6584 (1)
Ba: B (Å^2)	0.739 (18)	0.86 (2)	0.91 (2)	1.05 (5)
S: x	0.0623 (4)	0.0621 (4)	0.0625 (2)	0.0624 (2)
S: y	1/4	1/4	1/4	1/4
S: z	0.1908 (4)	0.1910 (4)	0.1911 (2)	0.1911 (2)
S: B (Å^2)	0.78 (6)	0.83 (5)	0.75 (3)	0.95 (5)
O1: x	0.4147 (9)	0.4142 (10)	0.4122 (7)	0.4118 (5)
O1: y	1/4	1/4	1/4	1/4
O1: z	0.3819 (11)	0.3897 (11)	0.394 (1)	0.3926 (7)
O1: B (Å^2)	1.8 (2)	1.33 (18)	1.06 (9)	2.03 (11)
O2: x	0.1901 (9)	0.1832 (9)	0.1823 (9)	0.1823 (5)
O2: y	1/4	1/4	1/4	1/4
O2: z	0.0543 (10)	0.0508 (11)	0.0494 (7)	0.0499 (7)
O2: B (Å^2)	0.64 (15)	0.90 (15)	1.64 (12)	1.65 (11)
O3: x	0.0792 (6)	0.0808 (6)	0.0801 (4)	0.0807 (3)
O3: y	0.0307 (7)	0.0293 (9)	0.0298 (7)	0.0291 (6)
O3: z	0.3073 (7)	0.3112 (7)	0.3114 (5)	0.3113 (4)
O3: B (Å^2)	0.31 (11)	0.65 (11)	1.08 (5)	1.34 (8)

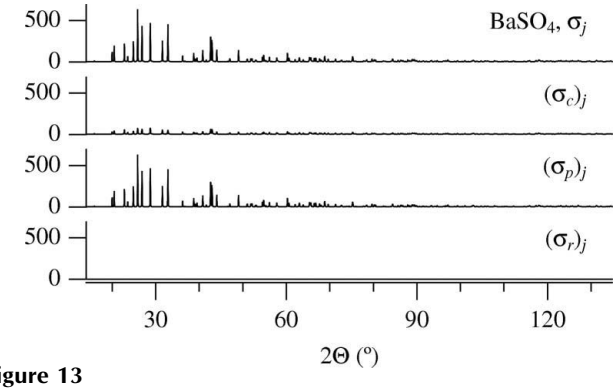

Figure 13
Total and component errors estimated for $BaSO_4$. $(\sigma_r)_j$ is estimated at zero.

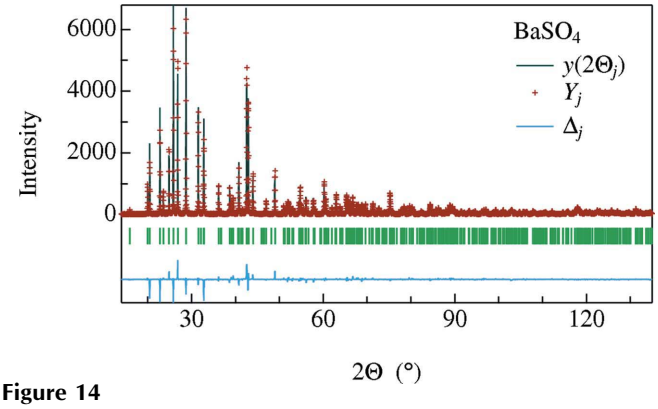

Figure 14
Final results of curve fitting for $BaSO_4$.

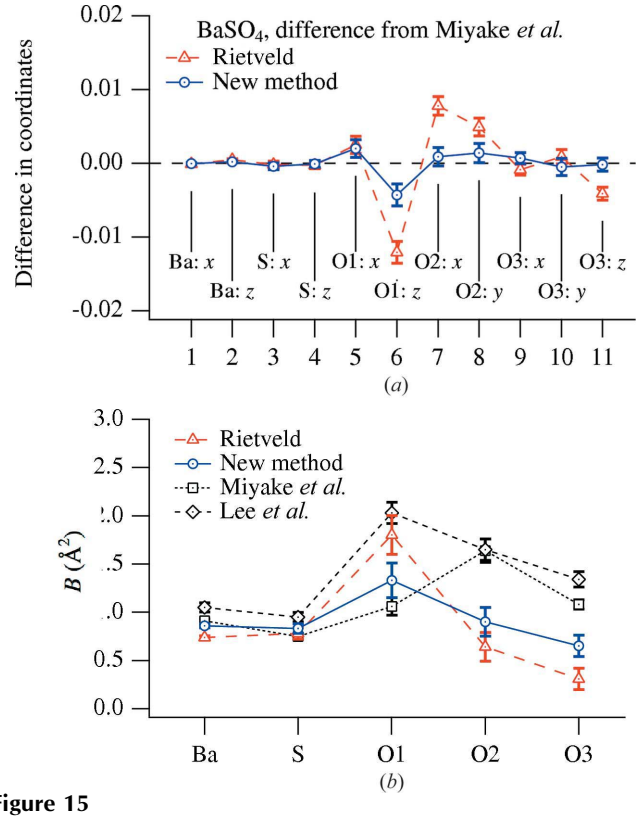

Figure 15
(*a*) Deviations of the fractional coordinates optimized by the Rietveld and new methods (which are, respectively, marked by triangles and circles) from those obtained by the single-crystal X-ray analysis by Miyake *et al.* (1978) for $BaSO_4$. (*b*) Isotropic atomic displacement parameters optimized by the Rietveld and new methods (triangles and circles, respectively) and equivalent isotropic atomic displacement parameters calculated from the single-crystal data (Miyake *et al.*, 1978; Lee *et al.*, 2005).

Effective multiplicities are plotted against 2Θ in Fig. 12. Fig. 13 shows calculated total errors σ_j and components $(\sigma_c)_j$, $(\sigma_p)_j$ and (σ_r), which are practically zero in $BaSO_4$.

The results of the final curve fitting to the powder diffraction data are plotted in Fig. 14. Table 3 lists reliability factors and structure parameters optimized by the Rietveld and new analytical methods. Standardized structure parameters, which were optimized by single-crystal X-ray analyses (Miyake *et al.*, 1978; Lee *et al.*, 2005), are also given in the table. Miyake *et al.* (1978) used a spherical crystal of barite, 0.15 mm in diameter, collected intensity data of 1398 independent reflections, and optimized structure parameters with R = 4.3%. Lee *et al.* (2005) used a crystal with dimensions of 0.33 × 0.25 × 0.15 mm, collected intensity data of 416 independent reflections, and optimized structure parameters with R = 2.54%.

(*a*) Differences in atomic coordinates between the structure refinements from the powder data and the single-crystal data (Miyake *et al.*, 1978) and (*b*) isotropic atomic displacement parameters, B, are plotted in Figs. 15(*a*) and 15(*b*), respectively. All the structure parameters, including the isotropic atomic displacement parameters, obtained by the new analytical method are significantly closer to the single-crystal data reported by Miyake *et al.* (1978) than those resulting from the Rietveld analysis.

Thus, our new method for structure refinement from powder diffraction data proved to be particularly effective for the diffraction data of $BaSO_4$, which seem to be strongly affected by particle statistics.

5. Conclusion

A new method to refine structure parameters, which can incorporate errors caused by particle statistics, has been developed and applied to the powder diffraction data of $Ca_5(PO_4)_3F$, $PbSO_4$ and $BaSO_4$. The refined structure parameters are significantly improved as compared with those obtained by conventional Rietveld refinement, especially in the case of the $BaSO_4$ data, where the effect of particle statistics is considerably marked.

References

Alexander, L., Klug, H. P. & Kummer, E. (1948). *J. Appl. Phys.* **19**, 742–753.
Antoniadis, A., Berruyer, J. & Filhol, A. (1990). *Acta Cryst.* A**46**, 692–711.
De Wolff, P. M. (1958). *Appl. Sci. Res.* **7**, 102–112.
Gelato, L. M. & Parthé, E. (1987). *J. Appl. Cryst.* **20**, 139–143.
Hill, R. J. (1992). *J. Appl. Cryst.* **25**, 589–610.
Ida, T. (2008). *J. Appl. Cryst.* **41**, 393–401.
Ida, T. (2011). *J. Appl. Cryst.* **44**, 911–920.
Ida, T., Goto, T. & Hibino, H. (2009). *J. Appl. Cryst.* **42**, 597–606.
Izumi, F. & Momma, K. (2007). *Solid State Phenom.* **130**, 15–20.
Lee, J.-S., Wang, H.-R., Iizuka, Y. & Yu, S.-C. (2005). *Z. Kristallgr.* **220**, 1–5.
Miyake, M., Minato, I., Morikawa, H. & Iwai, S. (1978). *Am. Mineral.* **63**, 506–510.
Momma, K. & Izumi, F. (2008). *J. Appl. Cryst.* **41**, 653–658.
Press, W. H., Flannery, B. P., Teukolsky, S. A. & Vetterling, W. T. (2007). *Numerical Recipes: the Art of Scientific Computing*, 3rd ed. Cambridge University Press.
Rietveld, H. M. (1969). *J. Appl. Cryst.* **2**, 65–71.
Rodriguez-Carvajal, J. (1993). *Physica B*, **192**, 55–69.
Sudarsanan, K., Mackie, P. E. & Young, R. A. (1972). *Mater. Res. Bull.* **7**, 1331–1338.
Toraya, H. (1990). *J. Appl. Cryst.* **23**, 485–491.
Toraya, H. (1998). *J. Appl. Cryst.* **31**, 333–343.
Toraya, H. (2000). *J. Appl. Cryst.* **33**, 95–102.
Young, R. A., Sakthivel, A., Moss, T. S. & Paiva-Santos, C. O. (1995). *J. Appl. Cryst.* **28**, 366–367.